Electron and fluorescence spectra of a water molecule irradiated by an x-ray free-electron laser pulse

Julia M. Schäfer,[1,2,*] Ludger Inhester,[1,†] Sang-Kil Son,[1,‡] Reinhold F. Fink,[2,§] and Robin Santra[1,3,‖]
[1]*Center for Free-Electron Laser Science, DESY, Notkestrasse 85, 22607 Hamburg, Germany*
[2]*Institute of Physical and Theoretical Chemistry, University of Tübingen, Auf der Morgenstelle 18, 72076 Tübingen, Germany*
[3]*Department of Physics, University of Hamburg, Jungiusstrasse 9, 20355 Hamburg, Germany*

(Received 22 February 2018; published 29 May 2018)

With the highly intense x-ray light generated by x-ray free-electron lasers (XFELs), molecular samples can be ionized many times in a single pulse. Here we report on a computational study of molecular spectroscopy at the high x-ray intensity provided by XFELs. Calculated photoelectron, Auger electron, and x-ray fluorescence spectra are presented for a single water molecule that reaches many electronic hole configurations through repeated ionization steps. The rich details shown in the spectra depend on the x-ray pulse parameters in a nonintuitive way. We discuss how the observed trends can be explained by the competition of microscopic electronic transition processes. A detailed comparison between spectra calculated within the independent-atom model and within the molecular-orbital framework highlights the chemical sensitivity of the spectral lines of multiple-hole configurations. Our results demonstrate how x-ray multiphoton ionization-related effects such as charge-rearrangement-enhanced x-ray ionization of molecules and frustrated absorption manifest themselves in the electron and fluorescence spectra.

DOI: 10.1103/PhysRevA.97.053415

I. INTRODUCTION

X-ray free-electron lasers (XFELs) [1] are emerging x-ray sources that stand out due to ultrashort pulse durations on the femtosecond timescale and unprecedented peak brilliances which are by many orders of magnitude higher than those of storage-ring-based synchrotron radiation sources [2,3]. The extremely bright and short pulses of XFELs are ideally suited for biomolecular imaging, where they have allowed for structure determination of macromolecules and viruses [4–8]. Aside from diffractive imaging, considerable attention has also been paid to the potential of XFELs with respect to spectroscopic applications [9,10]. The capability of XFELs to provide ultrashort pulses has enabled novel time-resolved spectroscopic experiments [11–14]. The work presented here is connected to the ultrahigh intensity of XFELs that has rendered a new regime in nonlinear x-ray spectroscopy accessible [15–19].

Concerning spectroscopy with molecules, the high XFEL intensity opens up new ways to create double core-hole states in molecules [20]. These double core-hole states have received significant attention, because in electron spectroscopy they show more sensitivity to the chemical environment than single core-holes [21–32]. Moreover, the appearance of multiple core vacancies may help to reduce the radiation damage in prospective single-molecule coherent diffractive imaging experiments because they temporarily reduce the x-ray absorption in the sample [2,33]. The electron and fluorescence spectra at high x-ray intensity mirror the underlying sequential multiphoton multiple ionization dynamics, i.e., the sequence of consecutive photoionization, Auger decay, and fluorescence decay steps that lead to the formation of the multiple core and valence vacancies. In this way, electron spectra at XFELs encode information on the radiation damage. On the other hand, they may help to investigate how double core-hole states can be created efficiently.

So far, the manifestation of ionization dynamics in spectra has only been investigated for a single xenon atom [34]. In molecules, the radiation damage can be significantly different from what one would expect for single atoms [35,36]. Here we analyze how the complex ionization dynamics at high x-ray intensity involving various different charge states manifests itself in the molecular photoelectron, Auger electron, and fluorescence spectra. We employ our x-ray molecular physics toolkit XMOLECULE [35,37] to calculate various spectra for a molecule exposed to an intense x-ray pulse. We choose a water molecule as a test system. In our approach [35] the time-dependent population of the electronic configurations is described with a rate equation model. For comparable applications of rate equations see Refs. [2,38–42]. In contrast to former approaches, where the number of absorbed photons was limited to two [20,43], the number of absorbed photons is not restricted and all possible electronic configurations, including multiple core- and valence-hole states, are taken into account. In our calculations, we employ x-ray pulses with Gaussian pulse envelopes of 1 fs, 5 fs, and 50 fs FWHM. We apply a photon energy of 1 keV throughout the work, which makes full ionization of the water molecule possible. The fluence is varied between 10^{10} photons/μm^2 and 10^{13} photons/μm^2. The number of soft-x-ray photons per pulse generated by currently operating XFELs is up to 10^{13} photons at LCLS AMO [44] and is

*julia.schaefer@cfel.de
†ludger.inhester@cfel.de
‡sangkil.son@cfel.de
§reinhold.fink@uni-tuebingen.de
‖robin.santra@cfel.de

expected to be up to 2×10^{14} photons at European XFEL SQS [45], and a typical focal area is few μm^2 for soft x-rays [2]. Thus, a peak fluence approaching 10^{13} photons/μm^2 is realistic. The outline of this article is as follows: Section II describes the computational methods used in this work. In Sec. III we show the resulting fluorescence, Auger electron and photoelectron spectra of H_2O when exposed to an intense x-ray pulse, and demonstrate how they imprint the multiphoton multiple ionization dynamics. In Sec. IV, we draw final conclusions.

II. COMPUTATIONAL METHODS

The interaction between an intense x-ray pulse and a water molecule may be described by a sequence of one-photon absorption steps. Every K-shell ionization is accompanied by the corresponding relaxation of the core hole, i.e., Auger decay or x-ray fluorescence. As has been described before [35], we model this ionization dynamics using the coupled rate equations,

$$\frac{d}{dt} P_I(t) = \sum_{I' \neq I} [\Gamma_{I' \to I}(t) P_{I'}(t) - \Gamma_{I \to I'}(t) P_I(t)], \quad (1)$$

where $P_I(t)$ is the time-dependent population of an electronic configuration I of the molecule. Each electronic configuration is characterized by a set of occupation numbers of the molecular orbitals. We take all possible configurations into account, in which the occupation numbers of the occupied orbitals of the neutral ground-state configuration can be zero, one, or two. For the water molecule this amounts to $3^5 = 243$ configurations. The quantities $\Gamma_{I \to I'}(t)$ in Eq. (1) are the rates for Auger or x-ray fluorescence decay from electronic configuration I to I', or the photoionization rates for the ionization process from I to I'. In contrast to the Auger and fluorescence decay rates, the photoionization rates $\Gamma_{I \to I'}(t)$ are time dependent, since they depend on the instantaneous x-ray flux density $J(t)$ at time t via

$$\Gamma_{I \to I'}(t) = \sigma_{I \to I'} J(t), \quad (2)$$

where $\sigma_{I \to I'}$ is the corresponding photoionization cross section.

The associated spectra are given by the time integral

$$F_\lambda(E) = \int_{-\infty}^{\infty} dt \sum_{I'} \sum_{I \neq I'} \Gamma_{I' \to I, \lambda}(t) f(E - E_{I' \to I}) P_{I'}(t), \quad (3)$$

where the summation over the rates $\Gamma_{I' \to I, \lambda}(t)$ is now restricted to a particular type of transition indicated by the additional index λ, which labels Auger transitions, fluorescence, or photoionization, respectively. The function $f(E - E_{I' \to I})$ is the corresponding line shape and $E_{I' \to I}$ is the transition energy for the considered transition. For simplicity we first bin here all spectra with 1-eV bins. Subsequently, all calculated spectra are convolved with a Gaussian function with 3 eV FWHM. The value of 3 eV constitutes an estimate of the spectral line broadening due to the interplay of finite lifetime effects, vibrational broadening, multiplet splitting, and dissociation effects, which are not included in our model. The effects of molecular dissociation and vibrational broadening are discussed in Sec. III E.

The photoionization cross sections and Auger decay and fluorescence rates are obtained from electronic structure calculations conducted with our toolkit XMOLECULE [37], which is based on the Hartree-Fock-Slater [46] model. As described in detail in Ref. [35], for every hole configuration that can be visited during the multiple x-ray ionization dynamics we calculate the molecular electronic structure and obtain a table of all possible photoionization cross sections, as well as Auger and fluorescence rates. We employ a minimal basis set constructed from numerical atomic orbitals. Specifically, for each molecular hole configuration we use basis functions that are taken from an atomic calculation for the respective core vacancy [37] conducted with the XATOM [40] toolkit. The obtained table of electronic transition rates and cross sections is then used to solve the coupled rate equations given in Eq. (1) by applying the 4th-order Runge-Kutta method. In addition, we integrate the time integral given in Eq. (3) in order to obtain the photoelectron, Auger electron, and fluorescence spectra.

For simplicity we neglect nuclear dynamics. Possible consequences of this approximation on the calculated spectra are discussed in Sec. III E. Our calculations do not contain shake-off and shake-up processes, either. Ejected photo- and Auger electrons are treated as noninteracting particles. Thus, phenomena such as the space-charge effect and postcollision interaction are not included. We think that these effects would have an overall minor impact on the spectra.

III. RESULTS AND DISCUSSION

A. Spectra of H_2O at high x-ray intensity

All spectra were calculated for a photon energy of 1 keV, which is above the ionization thresholds of all electronic configurations of H_2O. Figure 1 shows spectra that are obtained for a water molecule exposed to an ultraintense x-ray pulse with a fluence of 10^{13} photons/μm^2. The pulse is assumed to have a Gaussian-shaped temporal profile of 5 fs FWHM. As one can see, the individual spectra show rich details with various transition lines, which encode information on the dynamics during the multiple ionization of the molecule.

In Fig. 1(a) the spectrum of K-shell photoelectrons is shown. It contains a multitude of signals at different kinetic energies, because in the course of multiple ionization of the molecule many different electronic configurations with different charge states are visited. On top of the figure, the labels indicate the transition classes with "$[k,v]$," where $k = 0,1,2$ is the number of K-shell electrons, and $v = 0, \ldots, 8$ is the number of valence electrons in the water molecule. With higher charge states the K-shell binding energy increases such that the photoelectron lines shift to lower kinetic energies. This effect groups the spectral lines into remarkably well-separated energy regions corresponding to different charge states. Figure 1(b) shows the spectrum of valence photoelectrons, which have a much higher kinetic energy than the K-shell photoelectrons. As already observed for the K-shell photoelectron signal, the photoelectron lines originating from the valence shell shift to lower kinetic energies with higher charge states. In Fig. 1(c) the spectrum of emitted Auger electrons is shown. As can be seen, the signals cover a broad energy range homogeneously, because of the large number of different Auger processes occurring in the course of ionization dynamics. The

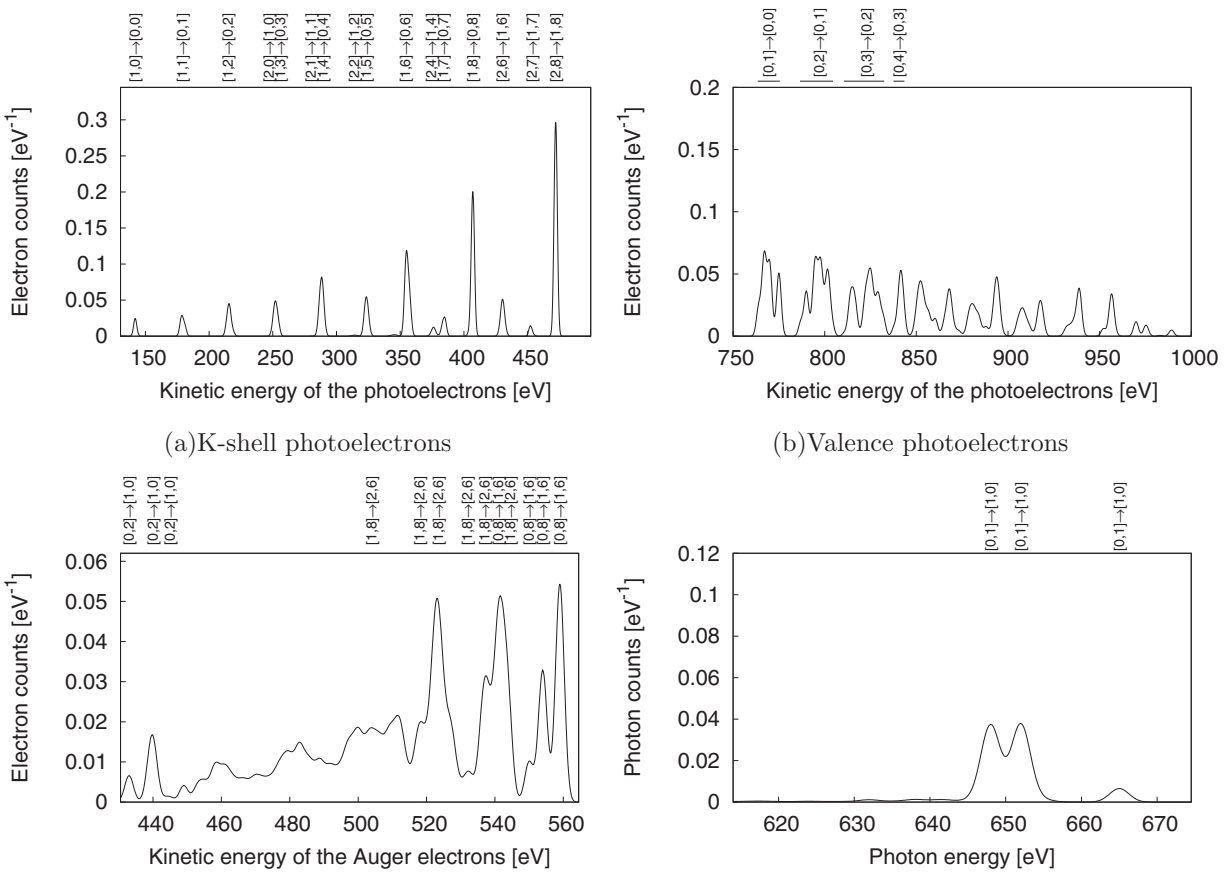

(a)K-shell photoelectrons (b)Valence photoelectrons

(c)Auger electrons (d)Fluorescence

FIG. 1. Photoelectron, Auger electron, and fluorescence spectra of a water molecule for a 1-keV x-ray pulse with Gaussian pulse envelope (5 fs FWHM) and a fluence of 10^{13} photons/μm^2. The labels indicate the transition classes with "$[k,v]$," where $k = 0,1,2$ is the number of K-shell electrons, and $v = 0,\ldots,8$ is the number of valence electrons in the water molecule.

fastest Auger electrons stem from refilling of a double core vacancy with eight valence electrons, whereas the slowest Auger electrons stem from refilling of a double core-hole in a +8 charged molecule. Figures 1(a) and 1(c) indicate that the K-shell photoelectron and Auger electron spectra overlap partially for the chosen photon energy of 1 keV. However, one could easily separate photoelectron and Auger electron spectra experimentally by employing a different photon energy. For example, a photon energy lowered by at least 50 eV would shift the kinetic energies of the photoelectrons below those of the Auger electrons. Figure 1(d) shows the x-ray fluorescence spectrum. Remarkably, lines from very specific valence-core combinations ([0,1]→[1,0]) have dominant contributions.

In order to understand the spectra in Fig. 1, one has to bear in mind that there are four competing processes at high x-ray intensity: K-shell photoionization, valence-shell photoionization, Auger decay, and fluorescence decay. At the chosen photon energy of 1 keV, K-shell photoionization is expected to be much stronger than valence-shell photoionization, since the K-shell photoionization cross section for the neutral water molecule (112.5 kb) is much higher than the valence-shell photoionization cross sections (0.3–3.8 kb). However, the overall contribution of valence ionization found here is remarkably high. For the considered case with a fluence of 10^{13} photons/μm^2 and a pulse duration of 5 fs, the calculated averaged number of ejected valence photoelectrons is 3.89, which is even slightly higher than the number of ejected K-shell photoelectrons (3.88) [see also Figs. 3(a) and 3(b)]. The largest contribution to the spectrum of valence photoelectrons in Fig. 1(b) is found at kinetic energies between 750 and 850 eV. We have identified these strong valence ionization contributions to stem from highly charged electronic configurations with a double core vacancy ([0,1], [0,2], [0,3], and [0,4]), which are reached under this high fluence and short pulse condition. For these states with few valence electrons left, Auger decay is either not possible ([0,1]), or the Auger lifetimes are larger than or comparable to the pulse duration of 5 fs (see Table I). Therefore, the relative

TABLE I. Total Auger lifetimes, calculated with our toolkit XMOLECULE [37], for the energetically lowest-lying occupation pattern of the electronic configurations [0,2], [0,3], and [0,4]. Molecular orbitals are sorted by their energy in the neutral ground state.

Electronic configuration	Occupation of the MOs	Associated total Auger lifetime in fs
[0,2]	02000	9.0
[0,3]	02100	5.4
[0,4]	02200	2.5

contribution of valence ionization for these configurations is higher than for other configurations.

The x-ray fluorescence spectrum almost exclusively contains [0,1]→[1,0] transitions, because for the [0,1] configurations Auger decay is impossible and therefore fluorescence is the only remaining decay process. For all other configurations, Auger decay dominates over fluorescence.

By analyzing the spectra, we demonstrate how to identify the underlying ionization dynamics. For the fast photoelectrons, the K-shell photoionization spectrum in Fig. 1 is dominated by the three peaks that are denoted with [2,8]→[1,8], [1,8]→[0,8], and [1,6]→[0,6]. Taking this into consideration, together with the high-intensity Auger line of [0,8]→[1,6] in Fig. 1(c), one can conclude that the dominant sequence for the first four steps in the ionization dynamics is

$$[2,8] \xrightarrow{\mathrm{P}} [1,8] \xrightarrow{\mathrm{P}} [0,8] \xrightarrow{\mathrm{A}} [1,6] \xrightarrow{\mathrm{P}} [0,6], \qquad (4)$$

where "P" denotes a K-shell photoionization and "A" stands for an Auger decay, respectively [38].

B. Molecular effects in the spectra at high x-ray intensity

Most computational methods simulating radiation damage in coherent diffractive imaging experiments [47–51] are based on the independent-atom model. In this concept the x-ray ionization of a polyatomic molecule is treated as if the molecule consisted of isolated atoms. However, it has recently been shown that at high x-ray fluences the ionization of a molecule is considerably enhanced compared to what is found for the independent-atom model [35,36]. This effect occurs due to molecular electron rearrangement that makes more electrons available for ionization on the heavier atoms with higher ionization cross sections. This has been called charge-rearrangement-enhanced x-ray ionization of molecules (CREXIM) [36]. In order to investigate how spectra of molecules at high x-ray intensity are affected by molecular features in contrast to purely atomic ones, we have conducted the same calculations as for the water molecule within the independent-atom model, i.e., for an isolated oxygen and two isolated hydrogen atoms.

Figure 2 shows a comparison between the spectra calculated in the molecular-orbital framework and in the independent-atom model. Here we use a pulse duration of 1 fs FWHM instead of 5 fs FWHM in Fig. 1. Effects of using a shorter pulse duration will be discussed in Sec. III C.

In the calculation for the independent atoms, the 1s electrons in the isolated hydrogen atoms exhibit a negligible probability of being ionized. As a result, the very high charge states of +9 and +10 are hardly ever reached in this framework. Accordingly, we can identify the transition [1,2]→[0,2] in the spectrum of the independent-atom calculation in Fig. 2(a) with ionization of the last electron of oxygen, whereas the hydrogen atoms stay neutral. The energy difference between the [1,0]→[0,0] transition in the molecular-orbital model and the [1,2]→[0,2] transition in the independent-atom model, which accounts for 31 eV (indicated in orange), is caused by the Coulomb attraction of the last electron by the two naked protons at the bond distance of the water molecule.

The first thing one notices in the K-shell photoelectron spectra is that the peaks of the same transitions (i.e., the same numbers of core and valence electrons in the molecule) are shifted in energy in the two approaches. They are connected by brackets in the figure. In the molecular-orbital calculation, the peak for the creation of the single core-hole ([2,8]→[1,8]) is shifted up by 7.0 eV in comparison to the corresponding peak in the independent-atom calculation. This chemical shift is due to the additional shielding of the nuclear charge by the two extra valence electrons, which decreases the 1s binding energy in the molecule. The chemical shift increases with rising number of valence holes: It amounts to 18.2 eV for the [2,7]→[1,7] transition and 27.2 eV for the [2,6]→[1,6] transition. This increment of the chemical shift illustrates that higher charges induce more rearrangement of the hydrogen electrons in the water molecule, and thus more shielding of the nuclear charge.

The strong chemical sensitivity of double core-hole states [20–32] is illustrated by the chemical shift of the [1,8]→[0,8] transition: It amounts to 19.2 eV, which is 2.7 times higher than for the [2,8]→[1,8] transition. Similarly to what we have seen for the single core-hole states, the chemical shift of the double core-hole states also increases with rising number of valence holes: 30.6 eV for [1,7]→[0,7], 40.4 eV for [1,6]→[0,6], and 44.4 eV for [1,5]→[0,5]. Interestingly, the chemical shift does not increase further for a valence electron number below four: 42.6 eV for [1,4]→[0,4], 43.4 eV for [1,3]→[0,3], and 42.8 eV for [1,2]→[0,2]. This demonstrates that at these high charge states the rearrangement of the hydrogen electrons towards the oxygen atom is completed.

In Fig. 2(b) the valence-shell photoelectron signal is shown, both in the molecular-orbital model and in the independent-atom model. As in the K-shell spectrum, energies of corresponding lines are shifted in the two models. The valence-shell photoelectron peaks are broader in the molecular calculation since, unlike the atomic oxygen 2p levels, the valence orbitals of molecular water are not degenerate. The signals involving the removal of the seventh and the eighth valence electron of a water molecule with double core-hole ([0,2]→[0,1] and [0,1]→[0,0]) have no equivalent in the calculation with independent atoms due to the negligible photoionization cross section of hydrogen.

The calculated Auger electron spectrum is shown for both models in Fig. 2(c). The spectrum obtained for independent atoms exhibits a clearer structure and better defined peaks than the spectrum resulting from the molecular calculation, due to the above-mentioned degeneracy of the O 2p levels in the atomic calculation. The spectral region with kinetic energies below 472 eV is not accessible in the independent-atom model. The x-ray fluorescence spectrum in Fig. 2(d) exclusively contains contributions from highly charged states, both in the molecular and atomic calculations. The most intense peaks in both models belong to the transitions in which the last accessible valence electron refills a double core-hole ([0,1]→[1,0] in the molecular calculation and [0,3]→[1,2] in the independent-atom calculation).

C. Pulse parameter dependence in the molecular calculation

Figures 1 and 2 show spectra for 5- and 1-fs pulse durations, respectively. In the molecular K-shell photoelectron spectrum the peak for the creation of the double core-hole with full valence shell ([1,8]→[0,8]) is more intense for the

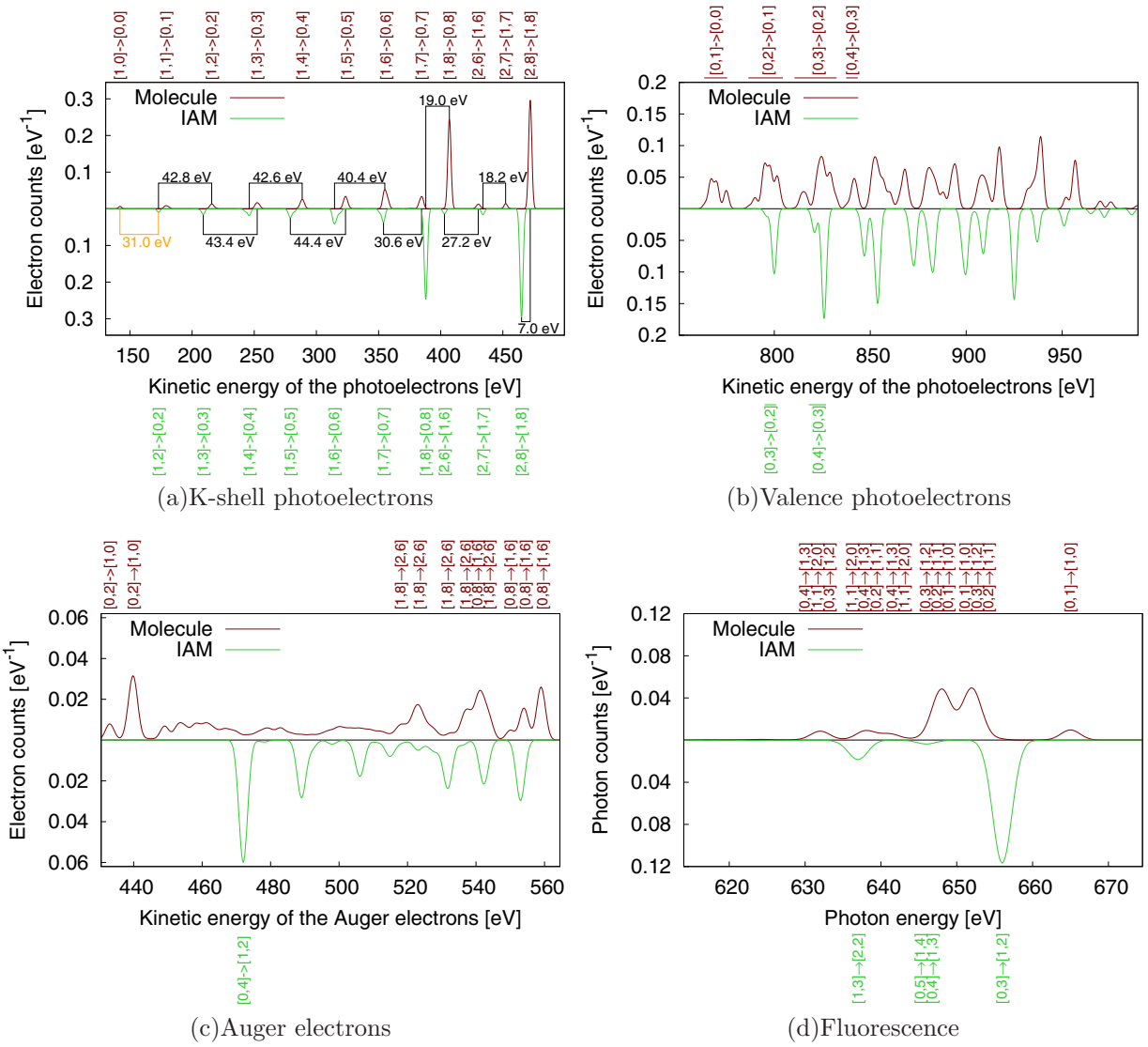

FIG. 2. Photoelectron, Auger electron, and fluorescence spectra of a water molecule in the molecular-orbital framework (brown upper line) and in the independent-atom model (IAM, green lower line) for a 1-keV x-ray pulse with Gaussian pulse envelope (1 fs FWHM) and a fluence of 10^{13} photons/μm^2. The labels indicate the transition classes with "$[k,v]$," where $k = 0,1,2$ is the number of K-shell electrons, and $v = 0,\ldots,8$ is the number of valence electrons in the water molecule.

1-fs pulse than for the 5-fs pulse. Moreover, the shorter pulse duration leads to more intensity in the molecular valence photoionization spectrum, especially in signals that correspond to configurations with few holes, at kinetic energies above 900 eV. The molecular Auger electron spectrum has a lower total intensity, but the Auger transitions with the highest possible charge ([0,2]→[1,0]) are more intense for the 1-fs than for the 5-fs pulse. The molecular fluorescence spectrum looks very similar for both 1 and 5 fs.

In order to further study the changes in the respective molecular and independent-atom spectra as a function of fluence and pulse duration, we now consider the integrated spectra, $\hat{F}_\lambda = \int_0^\infty dE\, F_\lambda(E)$, i.e., the total abundance of K-shell photoelectrons, valence-shell photoelectrons, Auger electrons, and fluorescence photons. In Fig. 3 the solid lines represent the integrated spectra calculated in the molecular-orbital framework for three different pulse durations, 1 fs, 5 fs, and 50 fs FWHM, as a function of fluence. The dotted lines give the corresponding quantities for the independent-atom model. In this section, we describe the general trends in Fig. 3, which are found both in the molecular and in the independent-atom calculation. In Sec. III D, we will then highlight the differences in the integrated spectra of both models.

The K-shell photoelectrons are shown in Fig. 3(a). As can be seen, the number of emitted K-shell photoelectrons increases with fluence and saturates for all pulse durations at a fluence of $\sim 10^{12}$ photons/μm^2. The saturation level is found to be lower for shorter pulse durations. Figure 3(b) contains the total number of valence photoelectrons. It increases with fluence for all pulse durations, but the rise is much slower as compared to the K-shell photoelectrons, and the curves saturate at much higher fluences. For the 1-fs pulse the total number of valence photoelectrons still increases considerably at 10^{13} photons/μm^2, whereas for the 50-fs pulse it is almost saturated for fluences

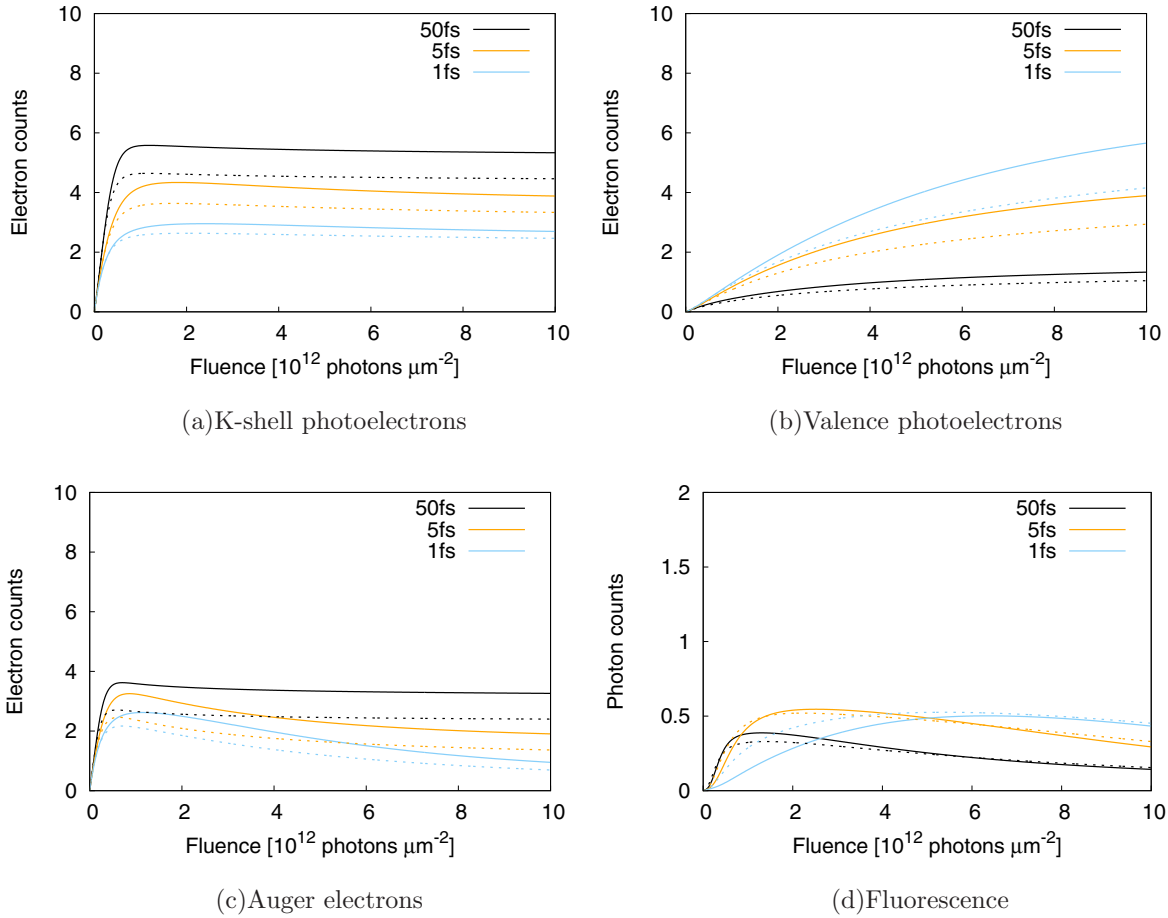

FIG. 3. Total number of K-shell photoelectrons, valence photoelectrons, Auger electrons, and fluorescence photons emitted by the water molecule as a function of fluence for an x-ray pulse with Gaussian pulse envelope for three different pulse durations (1 fs, 5 fs, and 50 fs FWHM). The solid lines show the molecular calculation, the dotted lines the independent-atom calculation.

larger than 3×10^{12} photons/μm^2. The level of saturation also depends on the pulse duration, but the dependence is reverse to the one for the K-shell photoelectrons: The longer the pulses, the fewer emitted valence photoelectrons.

The integrated number of Auger electrons is given in Fig. 3(c). Resembling the number of K-shell photoelectrons, the number of Auger electrons rapidly increases with fluence, but it saturates only for the 50-fs pulse. For the two shorter pulses it decreases with fluence for values larger than 10^{12} photons/μm^2. Similarly to the K-shell photoelectron case, longer pulses yield more Auger electrons than shorter pulses, but the differences with respect to pulse duration are less pronounced than in the trend for the K-shell photoelectrons. In Fig. 3(d), the number of emitted fluorescence photons is shown. Interestingly, it shows a nonmonotonic behavior with respect to the fluence for all three pulse durations considered here. For low fluences, the fluorescence signal increases, and it decreases again for very high fluences. The positions and the heights of the maximum value are different for the three pulse durations. For the 50-fs pulse, the fluorescence signal increases fastest and reaches a maximum at 10^{12} photons/μm^2. For the shorter pulses, it increases less rapidly and the maximum is reached at higher fluences (2×10^{12} photons/μm^2 for 5-fs, and 6×10^{12} photons/μm^2 for 1-fs pulse duration).

The fluence and pulse duration dependence of the integrated spectral intensities in the molecular calculation can be understood from the competition of the underlying microscopic electronic transition processes. If one sums together the total number of emitted electrons in the molecular calculation (photoelectrons and Auger electrons), one realizes that at a fluence of 10^{12} photons/μm^2, nearly all ten electrons of the water molecule are ionized, most drastically for the 50-fs pulse where on average 9.60 electrons are removed. Since there are only very few electrons in the molecule left for further ionization, the number of photoelectrons and Auger electrons saturates for high fluences. At very high x-ray intensity, the K-shell ionization rate can be larger than the corresponding Auger decay rate. In this regime, a significant amount of double K-shell vacancies is produced. At the same time, the amount of K-shell ionization is effectively reduced, if the pulse duration is shorter than the time to refill the K-shell vacancies by an Auger process. This phenomenon has become known as intensity-induced x-ray transparency [2] or frustrated absorption effect [33]. It explains why at the same fluence fewer K-shell photoelectrons are produced with a shorter pulse duration in Fig. 3(a).

The suppression of K-shell ionization with shorter pulses also leads to a reduction of the total number of Auger electrons

in Fig. 3(c). For the valence photoelectrons the opposite effect is seen: Since there is less Auger decay for a shorter pulse, more valence electrons stay in the valence shell and, thus, for a shorter pulse more valence electrons are exposed to the fluence and subsequently more of them are ionized as compared to the longer pulse case. Figures 3(b) and 3(c) reveal that for the 1- and 5-fs pulses valence ionization and Auger decay compete. At fluences larger than 10^{12} photons/μm^2, valence ionization dominates over Auger decay and therefore the amount of Auger electrons decreases as the fluence increases.

Understanding the behavior of the fluorescence signal requires special consideration: As we have seen in Fig. 1(d), the dominant part of the fluorescence stems from highly charged electronic configurations, which have very low Auger decay rates. Thus, the total amount of fluorescence increases rapidly with the population in these highly charged configurations, and therefore with rising fluence. For very high fluences, however, the rates of valence ionization start to be comparable with the fluorescence rates and therefore the fluorescence intensity decreases again.

D. Differences in the integrated spectra between the molecular and independent-atom calculations

As can be seen in Figs. 3(a) and 3(c), the total numbers of K-shell photoelectrons and Auger electrons are lower for the independent-atom model (dotted lines) than for the molecular calculation (solid lines). In the molecular case, the two additional electrons in the water molecule provided by the hydrogen atoms can be efficiently ionized by CREXIM through K-shell ionization and Auger decay. The difference between the molecular and the independent-atom calculations in the number of K-shell photoelectrons and Auger electrons is largest for the 50-fs pulse, where it maximally amounts to about one K-shell electron and one Auger electron. For the shorter pulses K-shell photoionization and Auger electron emission are less strongly enhanced due to molecular electron rearrangement. The numbers of valence photoelectrons [Fig. 3(b)] for the molecular calculation and the independent-atom calculation are very similar for the 50-fs pulse. Here, the molecular rearrangement shows little effect.

For the shorter pulses, however, valence ionization is considerably enhanced in the molecular calculation compared to the independent-atom model. Remarkably, these data suggest that molecular ionization enhancement may not only take place through providing more electrons for the Auger decays that help to refill the K-shell vacancy, but also via photoionization of valence electrons after charge rearrangement. This aspect has not been reported in previous works about enhanced x-ray ionization in molecules [35,36], because only hard x-ray radiation was considered where valence photoionization is negligible. For the soft x-ray radiation considered here, direct photoionization for valence electrons is not negligible anymore, and it becomes dominant when the valence photoionization rates become larger than the Auger transition rates. Note that the photoionization cross section of H_2O in the configuration [0,1] amounts to 3.6 kb (averaged over the four valence orbitals, in which the one electron may be found). This value is much larger than the photoionization cross section of H1s, 0.011 kb, in the independent-atom model. In this way, molecular electron rearrangement enhances the total molecular ionization via increasing the number of x-ray-accessible valence photoelectrons shown in Fig. 3(b). This effect becomes smaller for longer pulse durations, for example, for the 50-fs case in our calculations.

In total, the contributions of enhanced direct valence ionization, enhanced K-shell photoionization, and subsequent Auger decay sum up to a molecular ionization enhancement of +2 for the maximum fluence, 10^{13} photons/μm^2, and all pulse durations considered here.

E. Effects of molecular dissociation and vibrational broadening

The motion of the nuclei is not included in our calculations since we want to put the focus on how the ionization dynamics manifest themselves, in principle, in the spectra, rather than precisely rendering the line shapes as they would emerge in an experiment and as it is discussed, e.g., in Ref. [31]. Moreover, since we explore the whole parameter space by varying pulse durations and scanning through fluences, the computation of the electronic structure and the transition rates for all occurring molecular geometries would cause a tremendous computational effort. Nevertheless, the line shapes might reveal interesting information on the Coulomb explosion of the molecule.

It is well established that molecules may undergo dissociation within the lifetime of a core-hole state [52], which, for the water molecule in a core excited state, has been demonstrated in Ref. [53]. Even for a very short pulse of 1 fs, the effect of nuclear motion is not completely negligible, since the protons are rapidly accelerated by the strong Coulomb repulsion forces. In order to give an upper estimate on the effect of nuclear motion on the smearing out of spectral lines, we calculate how much the binding energy of the electrons is reduced due to Coulombic attraction between the electrons on the oxygen atom and the protons if one takes into account that the protons move away from the positively charged oxygen ion due to Coulomb repulsion. We calculate the energy shift of the spectral lines for instantaneous charges of the oxygen atom of +4 and the extreme case of +8. For a 1-fs pulse we expect a maximum shift of the spectral lines of $+7$ eV and $+11$ eV, and for a 5-fs pulse the maximum shift is $+24$ eV and $+26$ eV for the charges +4 and +8, respectively. The upper limit for the shift is $+31$ eV, which is the result if the protons are so far away from the oxygen atom that the Coulomb attraction between electrons and protons becomes negligible.

These results tell us that the incorporation of nuclear motion would further increase the chemical shift. Nuclear dynamics may alter the shape and position of the spectral lines. However, we expect the impact on the ionization dynamics to be rather small, because the total Auger decay rates for the water molecule are rather insensitive to the geometry [35,43,54], and photoionization (core and valence) happens predominantly on the oxygen atom, on which the electron density quickly concentrates with higher charge states. Therefore, we think that the area under the respective peaks is not sensitive to nuclear dynamics.

A second effect we have so far neglected in the calculated spectra is vibrational broadening. Since the hydrogen-oxygen bond length in the vibrational ground state of H_2O has a

distribution of finite width (standard deviation of $\sigma = 0.07$ Å), the electronic transition lines are broadened considerably due to the large slope of the dissociating potential energy surfaces (here approximated by Q/r, where Q is the charge of the oxygen atom and r is the O-H distance). For an oxygen charge of +4 this would yield a spectral broadening of 10.4 eV FWHM, and for an oxygen charge of +8 the vibrational broadening amounts to 20.7 eV FWHM. Hence, the spectral features are smeared out and are considerably broader when the system acquires a higher charge state. For the K-shell photoelectron spectra, where the lines for different numbers of holes are well separated, we still think that the individual lines can be identified.

IV. CONCLUSIONS

In this work, we extend the XMOLECULE toolkit to generate photoelectron, Auger electron, and x-ray fluorescence spectra at high x-ray intensity. The computational scheme is based on efficient molecular electronic structure calculations that allow us to take all possible multiple-hole configurations into account. After solving coupled rate equations, the time-dependent populations of the electronic configurations are obtained and spectra corresponding to each process are calculated. In our calculations a photon energy of 1 keV, pulse durations of 1 fs, 5 fs, and 50 fs, and fluences between 10^{10} photons/μm^2 and 10^{13} photons/μm^2 are assumed.

The results show that the K-shell photoelectron spectrum of H_2O at high x-ray intensity is remarkably well ordered, despite the extreme conditions. Interestingly, the chemical shift of double core-hole states is found to increase as a function of the number of valence holes, until it saturates at approximately 43 eV for a number of three or more valence holes, which indicates that at these high charge states the rearrangement of the hydrogen electrons towards the oxygen atom is completed. In consideration of the photon energy of 1 keV, a notable contribution of valence photoionization is found, which can be mainly assigned to highly charged states. The Auger electron spectrum is found to consist of a broad block nearly continuously covering the range between 440 and 560 eV. Similar to the valence photoelectron spectrum, strong signals in the fluorescence spectrum arise from highly charged configurations, with the largest contribution from molecules with only one remaining valence electron. The integrated spectra reveal that short pulses yield fewer K-shell photoelectrons and fewer Auger electrons than long pulses, but more valence photoelectrons. This behavior is identified as a manifestation of frustrated absorption in the spectra.

The recently found molecular ionization enhancement at high x-ray intensity due to molecular electron rearrangement is reflected in almost equal shares in the K-shell photoelectron spectrum and in the Auger electron spectrum of the water molecule. For soft x-ray pulses our findings suggest that valence photoionization may directly be enhanced through rearrangement of electrons in the molecule in the case of shorter pulses. This extends previous work on molecular ionization enhancement [35,36], where only hard x-rays were considered.

Further investigations may include nuclear dynamics, since nuclei in highly ionized molecules move very fast and this may leave interesting fingerprints in the spectra, especially in combination with longer pulses. The chemical shift in highly ionized molecules, with a focus on the comparison of double core-hole states with triple and quadruple core-hole states, should also be of interest for future work.

ACKNOWLEDGMENTS

J.M.S. thanks the EH-Stiftung for financial support. R.S. thanks the Deutsche Forschungsgemeinschaft for support through Grant No. SFB 925.

[1] B. W. J. McNeil and N. R. Thompson, X-ray free-electron lasers, Nat. Photonics **4**, 814 (2010).

[2] L. Young, E. P. Kanter, B. Krässig, Y. Li, A. M. March, S. T. Pratt, R. Santra, S. H. Southworth, N. Rohringer, L. F. DiMauro, G. Doumy, C. A. Roedig, N. Berrah, L. Fang, M. Hoener, P. H. Bucksbaum, J. P. Cryan, S. Ghimire, J. M. Glownia, D. A. Reis, J. D. Bozek, C. Bostedt, and M. Messerschmidt, Femtosecond electronic response of atoms to ultra-intense X-rays, Nature (London) **466**, 56 (2010).

[3] N. Rohringer, D. Ryan, R. A. London, M. Purvis, F. Albert, J. Dunn, J. D. Bozek, C. Bostedt, A. Graf, R. Hill, S. P. Hau-Riege, and J. J. Rocca, Atomic inner-shell x-ray laser at 1.46 nanometres pumped by an x-ray free-electron laser, Nature (London) **481**, 488 (2012).

[4] R. Neutze, R. Wouts, D. van der Spoel, E. Weckert, and J. Hajdu, Potential for biomolecular imaging with femtosecond x-ray pulses, Nature (London) **406**, 752 (2000).

[5] H. N. Chapman, A. Barty, M. J. Bogan, S. Boutet, M. Frank, S. P. Hau-Riege, S. Marchesini, B. W. Woods, S. Bajt, W. H. Benner, R. A. London, E. Plönjes, M. Kuhlmann, R. Treusch, S. Düsterer, T. Tschentscher, J. R. Schneider, E. Spiller, T. Möller, C. Bostedt *et al.*, Femtosecond diffractive imaging with a soft-X-ray free-electron laser, Nat. Phys. **2**, 839 (2006).

[6] M. M. Seibert, T. Ekeberg, F. R. N. C. Maia, M. Svenda, J. Andreasson, O. Jönsson, D. Odić, B. Iwan, A. Rocker, D. Westphal, M. Hantke, D. P. DePonte, A. Barty, J. Schulz, L. Gumprecht, N. Coppola, A. Aquila, M. Liang, T. A. White, A. Martin *et al.*, Single mimivirus particles intercepted and imaged with an X-ray laser, Nature (London) **470**, 78 (2011).

[7] L. Redecke, K. Nass, D. P. DePonte, T. A. White, D. Rehders, A. Barty, F. Stellato, M. Liang, T. R. M. Barends, S. Boutet, G. J. Williams, M. Messerschmidt, M. M. Seibert, A. Aquila, D. Arnlund, S. Bajt, T. Barth, M. J. Bogan, C. Caleman, T.-C. Chao *et al.*, Natively inhibited trypanosoma brucei cathepsin B structure determined by using an x-ray laser, Science **339**, 227 (2013).

[8] T. R. M. Barends, L. Foucar, S. Botha, R. B. Doak, R. L. Shoeman, K. Nass, J. E. Koglin, G. J. Williams, S. Boutet,

M. Messerschmidt, and I. Schlichting, *De novo* protein crystal structure determination from X-ray free-electron laser data, Nature (London) **505**, 244 (2014).

[9] S. Bernitt, G. V. Brown, J. K. Rudolph, R. Steinbrügge, A. Graf, M. Leutenegger, S. W. Epp, S. Eberle, K. Kubiček, V. Mäckel, M. C. Simon, E. Träbert, E. W. Magee, C. Beilmann, N. Hell, S. Schippers, A. Müller, S. M. Kahn, A. Surzzhykov, Z. Harman *et al.*, An unexpectedly low oscillator strength as the origin of the Fe XVII emission problem, Nature (London) **492**, 225 (2012).

[10] J. Kern, R. Alonso-Mori, R. Tran, J. Hattne, R. J. Gildea, N. Echols, C. Glöckner, J. Hellmich, H. Laksmono, R. G. Sierra, B. Lassalle-Kaiser, S. Koroidov, A. Lampe, G. Han, S. Gul, D. DiFiore, D. Milathianaki, A. R. Fry, A. Miahnahri, D. W. Schafer *et al.*, Simultaneous femtosecond x-ray spectroscopy and diffraction of photosystem II at room temperature, Science **340**, 491 (2013).

[11] H. T. Lemke, C. Bressler, L. X. Chen, D. M. Fritz, K. J. Gaffney, A. Galler, W. Gawelda, K. Haldrup, R. W. Hartsock, H. Ihee, J. Kim, K. H. Kim, J. H. Lee, M. M. Nielsen, A. B. Stickrath, W. Zhang, D. Zhu, and M. Cammarata, Femtosecond x-ray absorption spectroscopy at a hard x-ray rree electron laser: Application to spin crossover dynamics, J. Phys. Chem. A **117**, 735 (2013).

[12] M. Beye, T. Anniyev, R. Coffee, M. Dell'Angela, A. Föhlisch, J. Gladh, T. Katayama, S. Kaya, O. Krupin, A. Møgelhøj, A. Nilsson, D. Nordlund, J. K. Nørskov, H. Öberg, H. Ogasawara, L. G. M. Pettersson, W. F. Schlotter, J. A. Sellberg, F. Sorgenfrei, J. J. Turner *et al.*, Selective Ultrafast Probing of Transient Hot Chemisorbed and Precursor States of CO on Ru(0001), Phys. Rev. Lett. **110**, 186101 (2013).

[13] M. Dell'Angela, T. Anniyev, M. Beye, R. Coffee, A. Föhlisch, J. Gladh, T. Katayama, S. Kaya, O. Krupin, J. LaRue, A. Møgelhøj, D. Nordlund, J. K. Nørskov, H. Öberg, H. Ogasawara, H. Öström, L. G. M. Pettersson, W. F. Schlotter, J. A. Sellberg, F. Sorgenfrei *et al.*, Real-time observation of surface bond breaking with an x-ray laser, Science **339**, 1302 (2013).

[14] W. Zhang, R. Alonso-Mori, U. Bergmann, C. Bressler, M. Chollet, A. Galler, W. Gawelda, R. G. Hadt, R. W. Hartsock, T. Kroll, K. S. Kjær, K. Kubiček, H. T. Lemke, H. W. Liang, D. A. Meyer, M. M. Nielsen, C. Purser, J. S. Robinson, E. I. Solomon, Z. Sun *et al.*, Tracking excited-state charge and spin dynamics in iron coordination complexes, Nature (London) **509**, 345 (2014).

[15] L. Schroedter, M. Müller, A. Kickermann, A. Przystawik, S. Toleikis, M. Adolph, L. Flückiger, T. Gorkhover, L. Nösel, M. Krikunova, T. Oelze, Y. Ovcharenko, D. Rupp, M. Sauppe, D. Wolter, S. Schorb, C. Bostedt, T. Möller, and T. Laarmann, Hidden Charge States in Soft-X-Ray Laser-Produced Nanoplasmas Revealed by Fluorescence Spectroscopy, Phys. Rev. Lett. **112**, 183401 (2014).

[16] S. M. Vinko, O. Ciricosta, B. I. Cho, K. Engelhorn, H.-K. Chung, C. R. D. Brown, T. Burian, J. Chalupský, R. W. Falcone, C. Graves, V. Hájková, A. Higginbotham, L. Juha, J. Krzywinski, H. J. Lee, M. Messerschmidt, C. D. Murphy, Y. Ping, A. Scherz, W. Schlotter *et al.*, Creation and diagnosis of a solid-density plasma with an x-ray free-electron laser, Nature (London) **482**, 59 (2012).

[17] B. Ziaja, Z. Jurek, N. Medvedev, S.-K. Son, R. Thiele, and S. Toleikis, Photoelectron spectroscopy method to reveal ionization potential lowering in nanoplasmas, J. Phys. B **46**, 164009 (2013).

[18] B. Rudek, S.-K. Son, L. Foucar, S. W. Epp, B. Erk, R. Hartmann, M. Adolph, R. Andritschke, A. Aquila, N. Berrah, C. Bostedt, J. Bozek, N. Coppola, F. Filsinger, H. Gorke, T. Gorkhover, H. Graafsma, L. Gumprecht, A. Hartmann, G. Hauser *et al.*, Ultra-efficient ionization of heavy atoms by intense X-ray free-electron laser pulses, Nat. Photonics **6**, 858 (2012).

[19] T. Tachibana, Z. Jurek, H. Fukuzawa, K. Motomura, K. Nagaya, S. Wada, P. Johnsson, M. Siano, S. Mondal, Y. Ito, M. Kimura, T. Sakai, K. Matsunami, H. Hayashita, J. Kajikawa, X.-J. Liu, E. Robert, C. Miron, R. Feifel *et al.*, Nanoplasma formation by high intensity hard x-rays, Sci. Rep. **5**, 10977 (2015).

[20] R. Santra, N. V. Kryzhevoi, and L. S. Cederbaum, X-ray Two-Photon Photoelectron Spectroscopy: A Theoretical Study of Inner-Shell Spectra of the Organic Para-Aminophenol Molecule, Phys. Rev. Lett. **103**, 013002 (2009).

[21] L. S. Cederbaum, F. Tarantelli, A. Sgamellotti, and J. Schirmer, On double vacancies in the core, J. Chem. Phys. **85**, 6513 (1986).

[22] M. Tashiro, M. Ehara, H. Fukuzawa, K. Ueda, C. Buth, N. V. Kryzhevoi, and L. S. Cederbaum, Molecular double core-hole electron spectroscopy for chemical analysis, J. Chem. Phys. **132**, 184302 (2010).

[23] J. P. Cryan, J. M. Glownia, J. Andreasson, A. Belkacem, N. Berrah, C. I. Blaga, C. Bostedt, J. Bozek, C. Buth, L. F. DiMauro, L. Fang, O. Gessner, M. Guehr, J. Hajdu, M. P. Hertlein, M. Hoener, O. Kornilov, J. P. Marangos, A. M. March, B. K. McFarland *et al.*, Auger Electron Angular Distribution of Double Core-Hole States in the Molecular Reference Frame, Phys. Rev. Lett. **105**, 083004 (2010).

[24] P. Lablanquie, T. P. Grozdanov, M. Žitnik, S. Carniato, P. Selles, L. Andric, J. Palaudoux, F. Penent, H. Iwayama, E. Shigemasa, Y. Hikosaka, K. Soejima, M. Nakano, I. H. Suzuki, and K. Ito, Evidence of Single-Photon Two-Site Core Double Ionization of C_2H_2 Molecules, Phys. Rev. Lett. **107**, 193004 (2011).

[25] N. Berrah, L. Fang, B. Murphy, T. Osipov, K. Ueda, E. Kukk, R. Feifel, P. van der Meulen, P. Salen, H. T. Schmidt, R. D. Thomas, M. Larsson, R. Richter, K. C. Prince, J. D. Bozek, C. Bostedt, S. Wada, M. N. Piancastelli, M. Tashiro, and M. Ehara, Double-core-hole spectroscopy for chemical analysis with an intense x-ray femtosecond laser, Proc. Natl. Acad. Sci. U.S.A. **108**, 16912 (2011).

[26] N. V. Kryzhevoi, R. Santra, and L. S. Cederbaum, Inner-shell single and double ionization potentials of aminophenol isomers, J. Chem. Phys. **135**, 084302 (2011).

[27] M. Tashiro, K. Ueda, and M. Ehara, Auger decay of molecular double core-hole state, J. Chem. Phys. **135**, 154307 (2011).

[28] N. V. Kryzhevoi, M. Tashiro, M. Ehara, and L. S. Cederbaum, Interatomic relaxation effects in double core ionization of chain molecules, J. Chem. Phys. **137**, 154316 (2012).

[29] M. Nakano, F. Penent, M. Tashiro, T. P. Grozdanov, M. Žitnik, S. Carniato, P. Selles, L. Andric, P. Lablanquie, J. Palaudoux, E. Shigemasa, H. Iwayama, Y. Hikosaka, K. Soejima, I. H. Suzuki, N. Kouchi, and K. Ito, Single Photon K^{-2} and $K^{-1}K^{-1}$ Double Core Ionization in C_2H_{2n} ($n = 1$–3), CO, and N_2 as a Potential New Tool for Chemical Analysis, Phys. Rev. Lett. **110**, 163001 (2013).

[30] G. Goldsztejn, T. Marchenko, R. Püttner, L. Journel, R. Guillemin, S. Carniato, P. Selles, O. Travnikova, D. Céolin, A. F. Lago, R. Feifel, P. Lablanquie, M. N. Piancastelli, F. Penent, and M. Simon, Double-Core-Hole States in Neon: Lifetime,

Post-Collision Interaction, and Spectral Assignment, Phys. Rev. Lett. **117**, 133001 (2016).

[31] S. Oberli, N. Sisourat, P. Selles, and S. Carniato, Time-dependent quantum description of molecular double-core-hole-state formation: Impact of the nuclear dynamics on sequential two-photon processes, Phys. Rev. A **97**, 013406 (2018).

[32] J. H. D. Eland, M. Tashiro, P. Linusson, M. Ehara, K. Ueda, and R. Feifel, Double Core Hole Creation and Subsequent Auger Decay in NH_3 and CH_4 Molecules, Phys. Rev. Lett. **105**, 213005 (2010).

[33] M. Hoener, L. Fang, O. Kornilov, O. Gessner, S. T. Pratt, M. Gühr, E. P. Kanter, C. Blaga, C. Bostedt, J. D. Bozek, P. H. Bucksbaum, C. Buth, M. Chen, R. Coffee, J. Cryan, L. DiMauro, M. Glownia, E. Hosler, E. Kukk, S. R. Leone *et al.*, Ultraintense X-Ray Induced Ionization, Dissociation, and Frustrated Absorption in Molecular Nitrogen, Phys. Rev. Lett. **104**, 253002 (2010).

[34] S.-K. Son and R. Santra, Monte Carlo calculation of ion, electron, and photon spectra of xenon atoms in x-ray free-electron laser pulses, Phys. Rev. A **85**, 063415 (2012).

[35] L. Inhester, K. Hanasaki, Y. Hao, S.-K. Son, and R. Santra, X-ray multiphoton ionization dynamics of a water molecule irradiated by an x-ray free-electron laser pulse, Phys. Rev. A **94**, 023422 (2016).

[36] A. Rudenko, L. Inhester, K. Hanasaki, X. Li, S. J. Robatjazi, B. Erk, R. Boll, K. Toyota, Y. Hao, O. Vendrell, C. Bomme, E. Savelyev, B. Rudek, L. Foucar, S. H. Southworth, C. S. Lehmann, B. Kraessig, T. Marchenko, M. Simon, K. Ueda *et al.*, Femtosecond response of polyatomic molecules to ultra-intense hard x-rays, Nature (London) **546**, 129 (2017).

[37] Y. Hao, L. Inhester, K. Hanasaki, S.-K. Son, and R. Santra, Efficient electronic structure calculation for molecular ionization dynamics at high x-ray intensity, Struct. Dyn. **2**, 041707 (2015).

[38] N. Rohringer and R. Santra, X-ray nonlinear optical processes using a self-amplified spontaneous emission free-electron laser, Phys. Rev. A **76**, 033416 (2007).

[39] M. G. Makris, P. Lambropoulos, and A. Mihelič, Theory of Multiphoton Multielectron Ionization of Xenon under Strong 93-eV Radiation, Phys. Rev. Lett. **102**, 033002 (2009).

[40] S.-K. Son, L. Young, and R. Santra, Impact of hollow-atom formation on coherent x-ray scattering at high intensity, Phys. Rev. A **83**, 033402 (2011).

[41] U. Lorenz, N. M. Kabachnik, E. Weckert, and I. A. Vartanyants, Impact of ultrafast electronic damage in single-particle x-ray imaging experiments, Phys. Rev. E **86**, 051911 (2012).

[42] S. Serkez, G. Geloni, S. Tomin, G. Feng, E. V. Gryzlova, A. N. Grum-Grzhimailo, and M. Meyer, Overview of options for generating high-brightness attosecond x-ray pulses and applications at the European XFEL, J. Opt. **20**, 024005 (2018).

[43] L. Inhester, C. F. Burmeister, G. Groenhof, and H. Grubmüller, Auger spectrum of a water molecule after single and double core ionization, J. Chem. Phys. **136**, 144304 (2012).

[44] K. R. Ferguson, M. Bucher, J. D. Bozek, S. Carron, J.-C. Castagna, R. Coffee, G. I. Curiel, M. Holmes, J. Krzywinski, J. Krzywinski, M. Messerschmidt, M. Minitti, A. Mitra, S. Moeller, P. Noonan, T. Osipov, S. Schorb, M. Swiggers, A. Wallace, J. Yin, and C. Bostedt, The atomic, molecular and optical science instrument at the Linac Coherent Light Source, J. Synchrotron Radiat. **22**, 492 (2015).

[45] T. Tschentscher, C. Bressler, J. Grünert, A. Madsen, A. P. Mancuso, M. Meyer, A. Scherz, H. Sinn, and U. Zastrau, Photon beam transport and scientific instruments at the European XFEL, Appl. Sci. **7**, 592 (2017).

[46] J. C. Slater, A simplification of the Hartree-Fock method, Phys. Rev. **81**, 385 (1951).

[47] M. Bergh, N. Tîmneanu, and D. van der Spoel, Model for the dynamics of a water cluster in an x-ray free electron laser beam, Phys. Rev. E **70**, 051904 (2004).

[48] Z. Jurek, G. Faigel, and M. Tegze, Dynamics in a cluster under the influence of intense femtosecond hard x-ray pulses, Eur. Phys. J. D **29**, 217 (2004).

[49] S. P. Hau-Riege, R. A. London, and A. Szoke, Dynamics of biological molecules irradiated by short x-ray pulses, Phys. Rev. E **69**, 051906 (2004).

[50] S. P. Hau-Riege, Nonequilibrium electron dynamics in materials driven by high-intensity x-ray pulses, Phys. Rev. E **87**, 053102 (2013).

[51] B. Ziaja, Z. Jurek, N. Medvedev, V. Saxena, S.-K. Son, and R. Santra, Towards realistic simulations of macromolecules irradiated under the conditions of coherent diffraction imaging with an x-ray free-electron laser, Photonics **2**, 256 (2015).

[52] O. Björneholm, M. Bässler, A. Ausmees, I. Hjelte, R. Feifel, H. Wang, C. Miron, M. N. Piancastelli, S. Svensson, S. L. Sorensen, F. Gel'mukhanov, and H. Ågren, Doppler Splitting of In-Flight Auger Decay of Dissociating Oxygen Molecules: The Localization of Delocalized Core Holes, Phys. Rev. Lett. **84**, 2826 (2000).

[53] I. Hjelte, M. N. Piancastelli, R. F. Fink, O. Björneholm, M. Bässler, R. Feifel, A. Giertz, H. Wang, K. Wiesner, A. Ausmees, C. Miron, S. L. Sorensen, and S. Svensson, Evidence for ultra-fast dissociation of molecular water from resonant Auger spectroscopy, Chem. Phys. Lett. **334**, 151 (2001).

[54] H. Ågren, A. Cesar, and V. Carravetta, On the constant resonance width approximation for core electron ionization, Chem. Phys. Lett. **139**, 145 (1987).